The Lamb wave bandgap variation of a locally resonant phononic crystal subjected to thermal deformation

Cite as: AIP Advances **8**, 055109 (2018); https://doi.org/10.1063/1.5026523
Submitted: 21 February 2018 • Accepted: 29 April 2018 • Published Online: 09 May 2018

Yun Zhu, Zhen Li and Yue-ming Li

The Lamb wave bandgap variation of a locally resonant phononic crystal subjected to thermal deformation

Yun Zhu, Zhen Li, and Yue-ming Li[a]
State Key Laboratory for Strength and Vibration of Mechanical Structures, Shaanxi Key Laboratory of Environment and Control for Flight Vehicle, School of Aerospace, Xi'an Jiaotong University, Xi'an 710049, China

(Received 21 February 2018; accepted 29 April 2018; published online 9 May 2018)

A study on dynamical characteristics of a ternary locally resonant phononic crystal (PC) plate (*i.e.*, hard scatterer with soft coating periodically disperse in stiff host matrix) is carried out in this paper. The effect of thermal deformation on the structure stiffness, which plays an important role in the PC's dynamical characteristics, is considered. Results show that both the start and the stop frequency of bandgap shift to higher range with the thermal deformation. In particular, the characteristics of band structure change suddenly at critical buckling temperature. The effect of thermal deformation could be utilized for tuning of phononic band structures, which can promote their design and further applications.
https://doi.org/10.1063/1.5026523

I. INTRODUCTION

A novel class of media (*i.e.*, phononic crystals (PCs)) characterized by having an elastic wave bandgap to prevent sound and elastic waves propagation, have been studied extensively since Kushwaha's work.[1] However, forming bandgaps within low frequencies is quite difficult due to the limitation of lattice constant in classic PCs. Liu *et al.*[2] did the pioneer works by proposing a locally resonant PC, in which the bandgap frequencies reduced at least one order lower than that formed by Bragg scattering mechanism. Furthermore, Chen *et al.*[3,4] studied a class of architecture-PCs with broad and multiple bandgaps. By comparison between the effective wavelength and PCs' structural periodicity, it's found that the coupling between Bragg scattering and local resonances forms the low-frequency bandgaps. With the elastic wave bandgaps, PCs have caught increasing attention in numerous applications, including vibration isolation, acoustic filters, and waveguides.[5–8] Hence, a series of studies have been carried out to investigate the tenability of bandgaps characteristics depending on physical properties, filling fraction, and so on.[9–13]

Furthermore, the influences of multiple physical fields on PCs have also been extensively studied. Yeh[14] proposed certain methods to control the bandgaps of PCs inserted electro rheological material through electric fields. Wang *et al.*[15–17] analyzed the magneto-electro-elastic coupling and the effects of the piezoelectricity and piezomagnetism on the band structures. Chen *et al.*[18] studied a class of architected PCs, which exhibits extreme Poisson's-ratio variations under uniaxial tension. The results indicate that the bandgaps of the PCs can be tuned by external mechanical loading. Cheng *et al.*[19] formed a one-dimensional PC plate by alternating strips of ferroelectric ceramic Ba0.7Sr0.3TiO3 and epoxy. They found that the width and position of Lamb wave bandgaps shift prominently with the increment of temperature. Chen[20] studied temperature-tuned omnidirectional reflection bands in a one-dimensional finite PC consisted of nitinol and epoxy. There exist notable changes in the band structures of PCs by considering the coupling among magnetic, electric, thermal and elastic phenomena.

[a]Electronic mail: liyueming@xjtu.edu.cn (Yue-ming Li).

However, their works are limited by only considering the effects of material properties on bandgaps characteristics. The stress and deformation induced by physics fields were neglected, which impact more predominantly on the dynamic characteristics of structure.[21,22] When the plate is subjected to thermal environment, the structure stiffness changes as a result of the variation of material properties and thermal stress.[23–25] These factors result in multiple effects to the structure stiffness and further affect the dynamic characteristics. Li *et al.*[26] found the bandgap of a PC plate being narrower and shifting to lower frequency by taking the softening effect of thermal stress into account. The influences of thermal deformation (the thermal buckling in particular) on the dynamic characteristics of the PCs are remarkable, dominating the band structure directly. However, relevant studies on thermal deformation effects are still meager so far.

In this paper, a locally resonant PC, which is an aluminium plate filled with methyl vinyl silicone rubber (VMQ) and lead cylinders periodically, is proposed. Finite element method is used to analyze the bandgaps and eigenmodes of the structure. Based on critical buckling temperature, the Lamb wave bandgaps variation range is divided into pre-bulking process and post-bulking process. The characteristics of Lamb wave bandgaps show a sluggish response to the increasing temperature during the pre-bulking process, while the stop band is more sensitive to temperature variation during the post-bulking process by considering the buckling deformation of PC structure.

II. MODEL AND COMPUTATION THEORY

In this paper, a locally resonant PC plate is considered to study the effect of the thermal deformation. The PC structure is comprised of an aluminium plate periodically filled with methyl vinyl silicone rubber (VMQ) and lead cylinders. Fig. 1 shows the unit cell of which the height of the plate h=2mm, the lattice constant a=40mm, the exterior radius of VMQ r_1=16mm, the inner radius of VMQ r_2=8mm. Material parameters are given in Table I.

Actually, the thermal effects on PCs band structures could be classified into three categories: thermal mechanical properties, thermal stress and thermal deformation. Cheng[19] and Chen[20] researched in thermal effects on PCs band structures adequately, but they mainly discussed thermal mechanical properties. Meanwhile, Li[26] studied the thermal stress effect preliminarily. In this paper, the thermal deformation effect on the band structure is discussed.

Considering thermal stress and thermal deformation, the whole stiffness of the PC plate could be decomposed into three parts: the conventional stiffness referring to initial model, the additional

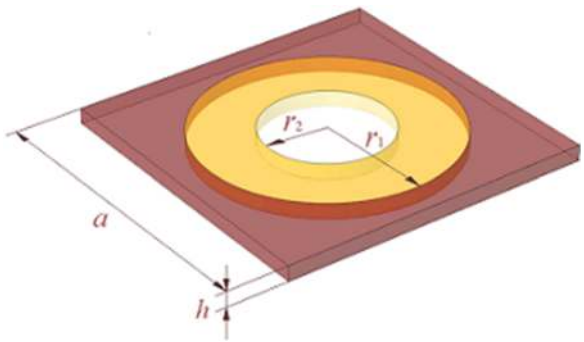

FIG. 1. Geometry of the unit cell.

TABLE I. Material parameters of the photonic crystal.

Material	Young modulus GPa	Poisson's ratio	Density kg/m^3	Thermal expansion coefficient 10^{-6}/K
aluminium	70	0.35	2700	23.6
VMQ	0.00214	0.49	1300	170
lead	17	0.42	11343	29.3

stiffness matrix induced by thermal stress, and the additional stiffness matrix induced by thermal deformation.[27] The dynamic function of the heated PC plate can be expressed by FEM as:

$$(K_0 + \Delta K_\sigma + \Delta K_d)U + M\ddot{U} = 0 \tag{1}$$

where,

M is the mass matrix;
U is the displacement vector;
K_0 is the stiffness matrix of the initial structure;
ΔK_σ is the additional stiffness matrix induced by thermal stress;
ΔK_d is the additional stiffness matrix induced by thermal deformation;

The detail of ΔK_σ has been given in Ref. 26. Here, to study the thermal deformation individually, the thermal stress and temperature tunable material properties, which have been studied,[19,20,26] are not considered during calculating the band structure. Hence, the dynamic equation (1) of the deformed PC plate could be expressed as:

$$(K_0 + \Delta K_d)U - \omega^2 MU = 0 \tag{2}$$

in which,

$$\begin{aligned}
\Delta K_d &= K_d - K_0 \\
&= \sum_e (K_d^e - K_0^e) \\
&= \sum_e \Big(\iiint_{\Omega_d} {B_d}^{\mathrm{T}} D B_d \mathrm{d}x\mathrm{d}y\mathrm{d}z - \iiint_{\Omega_0} {B_0}^{T} D B_0 \mathrm{d}x\mathrm{d}y\mathrm{d}z \Big) \\
&= \sum_e \int_{-1}^{1}\int_{-1}^{1}\int_{-1}^{1} ({B_d}^{\mathrm{T}} D B_d |J_d| - {B_0}^{T} D B_0 |J_0|)\mathrm{d}\xi\mathrm{d}\eta\mathrm{d}\zeta \\
&= \sum_e \int_{-1}^{1}\int_{-1}^{1}\int_{-1}^{1} ({N_d}^{\mathrm{T}} L^{\mathrm{T}} D L N_d |J_d| - {N_0}^{T} L^{\mathrm{T}} D L N_0 |J_0|)\mathrm{d}\xi\mathrm{d}\eta\mathrm{d}\zeta
\end{aligned} \tag{3}$$

ω is the circular frequency;
K_d is the stiffness matrix of the deformed structure;
Ω denotes the area of an element;
D is the element elastic matrix;
B is the element strain matrix;

$J = \begin{bmatrix} \frac{\partial x}{\partial \xi} & \frac{\partial y}{\partial \xi} & \frac{\partial z}{\partial \xi} \\ \frac{\partial x}{\partial \eta} & \frac{\partial y}{\partial \eta} & \frac{\partial z}{\partial \eta} \\ \frac{\partial x}{\partial \zeta} & \frac{\partial y}{\partial \zeta} & \frac{\partial z}{\partial \zeta} \end{bmatrix}$ is the Jacobian matrix;

$L = \begin{bmatrix} \frac{\partial}{\partial x} & 0 & 0 & \frac{\partial}{\partial y} & 0 & \frac{\partial}{\partial z} \\ 0 & \frac{\partial}{\partial y} & 0 & \frac{\partial}{\partial x} & \frac{\partial}{\partial z} & 0 \\ 0 & 0 & \frac{\partial}{\partial z} & 0 & \frac{\partial}{\partial y} & \frac{\partial}{\partial x} \end{bmatrix}^{\mathrm{T}}$ is the differential operator;

N is the element shape function matrix;
x, y, z are the global coordinate respectively;

ξ, η, ζ are the iso-parametric coordinate respectively;
The subscript d and 0 denote the deformed and initial state respectively;
The superscript e denotes an element.

In an element, D is defined by mechanical properties; N is defined by x_o, x_d, the nodal global coordinate. Here, the mechanical properties are considered as constants. And x_0 is given by FEM discretization. However, x_d, the nodal global coordinate of the deformed PC plate, is the unknown quantity. The relationship between x_0 and x_d is

$$x_d = x_0 + u_t \tag{4}$$

where, u_T is the nodal thermal displacement.

In order to regenerate the finite element model by taking x_d to replace x_0, u_T could be obtained.

A. Thermal deformation

In this paper, we use FEM software, ABAQUS, to solve the thermal-elastic equilibrium equation:

$$Ku_t = P \tag{5}$$

in which, $P = \sum_e \iiint_{\Omega_0} {B_0}^T D\varepsilon_t \mathrm{d}x\mathrm{d}y\mathrm{d}z$ is the thermal load matrix; ε_t is the thermal strain vector, for isotropic materials

$$\varepsilon_t = \alpha \Delta \mathrm{T} \begin{bmatrix} 1 & 1 & 1 & 0 & 0 & 0 \end{bmatrix} \tag{6}$$

The periodic boundary condition is applied to the unit cell of PC plate during the calculating of the thermal deformation. The unit cell is divided into five parts: the inner zone 1, and the four boundaries 2, 3, 4, 5 as shown in Fig. 2.

Thus, the nodal thermal displacement of the whole FEM model could be reduced as:

$$u_t = Su_t' \tag{7}$$

in which,

$u_t = \left[{u_{t,1}}^{\mathrm{T}}, {u_{t,2}}^{\mathrm{T}}, {u_{t,3}}^{\mathrm{T}}, {u_{t,4}}^{\mathrm{T}}, {u_{t,5}}^{\mathrm{T}} \right]^{\mathrm{T}}$ is the nodal thermal displacement;

$S = \begin{bmatrix} I & 0 & 0 & 0 & 0 \\ 0 & I & 0 & I & 0 \\ 0 & 0 & I & 0 & I \end{bmatrix}^{\mathrm{T}}$ is the transform matrix;

$u_t' = \left[{u_{t,1}}^{\mathrm{T}}, {u_{t,2}}^{\mathrm{T}}, {u_{t,3}}^{\mathrm{T}} \right]^{\mathrm{T}}$ is the reduced thermal displacement;

Hence, the Eq. (5) could be transformed to

$$K'u_t' = P' \tag{8}$$

in which, $K' = S^{\mathrm{T}}KS$, $M' = S^{\mathrm{T}}P$.

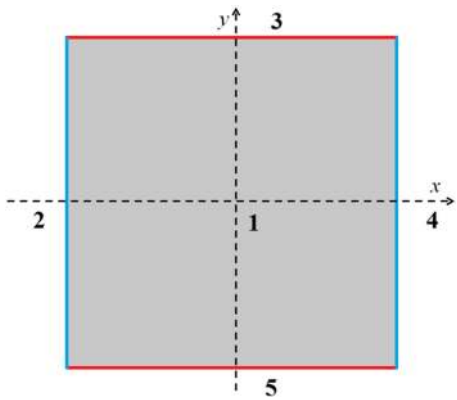

FIG. 2. Five parts of the unit cell.

Furthermore, the large deformation of the PC plate caused by thermal buckling are also concerned in this paper. To study the dependence of thermal buckling and post-buckling behavior with the band structure of PC plate, we use the method in Ref. 28, which could be separated to two steps. In step one, the calculations of linear critical (critical buckling temperature) and linear buckling modes are carried out. In step two, the thermal post-buckling performances of the PC plate described below are obtained by Riks method. In the analysis of the post-buckling, the initial destabilization of the structure dominates the large deformation. To obtain the configuration of buckling plate, the first-order mode of buckling is taken as initial destabilization.

B. Elastic wave band structure

According to Bloch-Floquet theorem, all fields are expressed as products of a periodic function times $\exp\left(-ik_x x - ik_y y\right)$. The unit cell is divided into 5 parts to applying Bloch-Floquet periodic conditions, as shown in Fig. 2. The displacement vector could be transformed to

$$U = S'U' \tag{9}$$

where,

$U = \left[{U_1}^{\mathrm{T}}, {U_2}^{\mathrm{T}}, {U_3}^{\mathrm{T}}, {U_4}^{\mathrm{T}}, {U_5}^{\mathrm{T}}\right]^{\mathrm{T}}$ is the nodal displacement vector;

$\overline{S} = \begin{bmatrix} I & 0 & 0 & 0 & 0 \\ 0 & I & 0 & \exp(-ik_x a)I & 0 \\ 0 & 0 & I & 0 & \exp\left(-ik_y a\right)I \end{bmatrix}^{\mathrm{T}}$ is the transform matrix;

$U' = \left[{U_1}^{\mathrm{T}}, {U_2}^{\mathrm{T}}, {U_3}^{\mathrm{T}}\right]^{\mathrm{T}}$ is the reduced nodal displacement vector;

$a = 0.04\mathrm{m}$ is the lattice constant.

And the Eq. (2) could be transformed to

$$(K_0{}' + \Delta K_d{}')U' - \omega^2 M'U' = 0 \tag{10}$$

in which, $K_0' = \overline{S}^{\mathrm{T}} K_0 \overline{S}$; $\Delta K_d' = \overline{S}^{\mathrm{T}} \Delta K_d \overline{S}$; $M' = \overline{S}^{\mathrm{T}} M \overline{S}$.

To obtain the band diagrams, any Bloch wave vector within the first Brillouin zone is considered and solved for the frequency of allowed modes by using FEM software, COMSOL. The band diagram describes the dispersion relationship between the frequency and Bloch wave vector.

III. NUMERICAL RESULTS AND ANALYSIS

A. Results of thermal deformation

The thermal deformation of the PC plate is obtained in this section. We set 0°C as the reference temperature (T_f) and increase the temperature load of the PC plate from 0°C to 160°C. The critical temperature of thermal buckling (T_c) is 142.92°C. Fig. 3 shows the buckling modes of the PC unit cell.

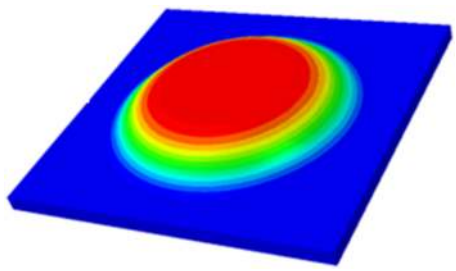

FIG. 3. Thermal buckling mode of the unit cell.

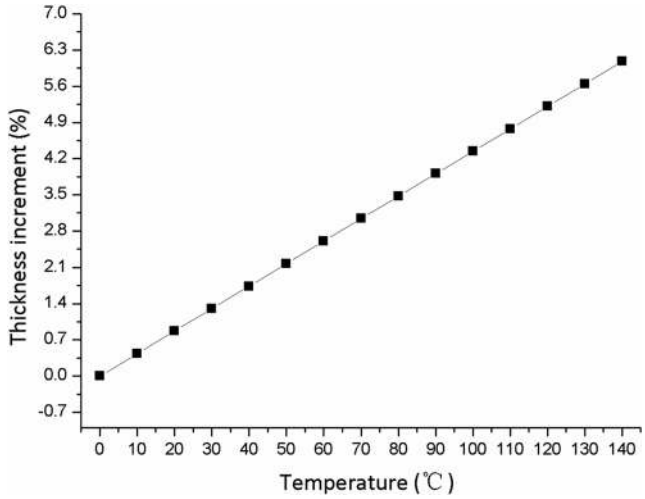

FIG. 4. The increment of the VMQ coating thickness with temperature rising.

In this paper, the thermal deformation behaviors of the PC are divided into two stages (the pre-buckling stage and the post-buckling stage) by the critical temperature. In the pre-buckling stage, the thermal deformation of the PC plate is linear and limited. Three parts of the PC plate expand and restrict each other during the heating process. Particularly, the VMQ coating thickens more significantly than the other parts because of its thermal expansion coefficient and Young modulus. Due to the limited thermal deformation of the pre-buckling plate unit cell, the increment of the VMQ coating thickness is used to scale the deformation degree, as shown in Fig. 4.

However, the unit cell configuration transforms remarkably, when the temperature reaches T_c. The VMQ coating is bended, and the lead core is deflected from the initial neutral plane. Fig. 5 shows the side view of the PC plate configuration at 143°C. Obviously, the VMQ coating transforms from an annular plate to an approximate truncated conical shell. To present the deformation degree of the unit cell intuitively, the transverse displacement of the observation point (pointed in Fig. 5) variation trend with temperature is shown in Fig. 6.

B. Band structure of the PC plate at 0°C

The first seven order bands of the PC structure at 0°C are shown in Fig. 7. The vertical axis is the frequency, and the horizontal axis is the reduced wave vector $k^* = k \cdot a/\pi$. k is the wave vector along the Brillouin zone (see in the insert of Fig. 7).

The propagations of three kinds of slab mode (anti-symmetric, symmetric and shear-horizontal modes) are supported in a finite thickness plate.[29] To estimate the Lamb wave bandgap, we make observation and analysis of the displacement vector fields in some vibration modes labeled which are given in Fig. 8. O_1 mode and O_2 mode (as shown in Figs. 8(a) and 8(b)) are symmetric mode (S_0 mode) and shear horizontal mode (SH_0 mode) respectively. O_3 mode, A mode and F mode (as shown in Figs. 8(c), 8(d), and 8(j)) are anti-symmetric modes (A_0 mode). B mode, E mode (as shown in Figs. 8(e) and 8(f)) are symmetric modes. C_1 mode, C_2 mode (as shown in Figs. 8(g) and 8(h)) are shear horizontal modes. D mode (as shown in Fig. 8(i)) is a torsional mode (T_0 mode). Meanwhile, A, B, C_1, C_2 and D mode could be assorted as locally resonant modes (LR modes). It indicates that the vibrations are centralized in the scatterers, while the vibration amplitude of the matrix is close to zero.

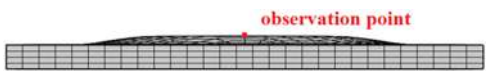

FIG. 5. Side view of the PC plate configuration (T=143°C).

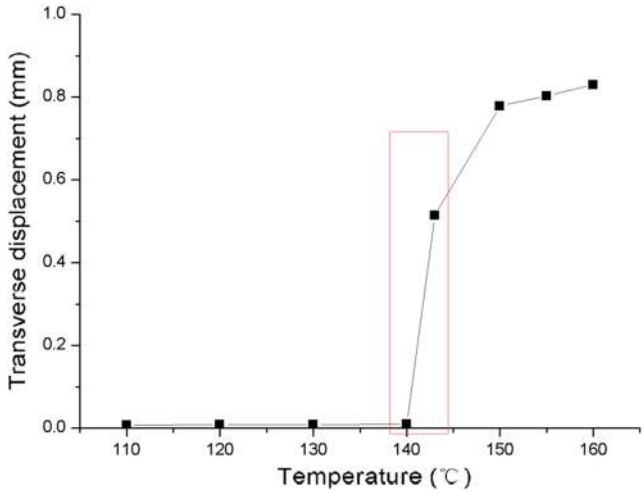

FIG. 6. Transverse displacement of the observation point variation trend with temperature.

These bands are divided into two parts: anti-symmetric modes or others (symmetric and shear-horizontal). Hence, there is an anti-symmetric Lamb wave bandgap (yellow area in Fig. 7) between 121.5 and 175.2 Hz. The S_0 mode and SH_0 mode in the bands are across the frequency range of the first-order anti-symmetric wave bandgap, which has no out-of-plane vibration component. Thus, this bandgap could also be recognized as an out-of-plane wave bandgap.[30]

The lower edge of this Lamb wave bandgap is depended on mode A. In mode A, the scatterer and the coating, which compose a mass-spring system, vibrate along z-axis while the matrix is almost static. The upper edge of the bandgap is depended on mode F. The matrix vibrates along z-axis in mode F. It means that the Lamb wave can propagate through the PC plate and the bandgap is cut off. Consequently, the Lamb wave bandgap is bounded by mode A and mode F.

C. Bandgap variation with temperature

Fig. 9 shows the band structures of the PC plate at 140°C and 143°C. Fig. 10 shows the bandgap variation with temperature rising at two stages. The range of bandgap shifts to higher frequency and the width of bandgap increases linearly at the pre-buckling stage. However, the thermal buckling behavior has remarkable effects on band structure. The bandgap shifts up and broadens rapidly at T_c.

To analyze this phenomenon, the PC plate unit cell is simplified as a mass-spring system. The VMQ coating acts as a spring mainly, while the aluminium plate and the lead core acts as mass blocks in this system. At the pre-buckling stage, the spring stiffness increases slowly with the VMQ

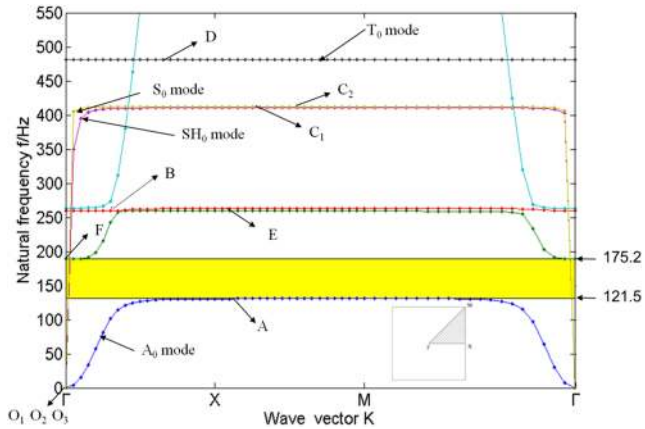

FIG. 7. Band structure of the locally resonant PC plate at 0°C.

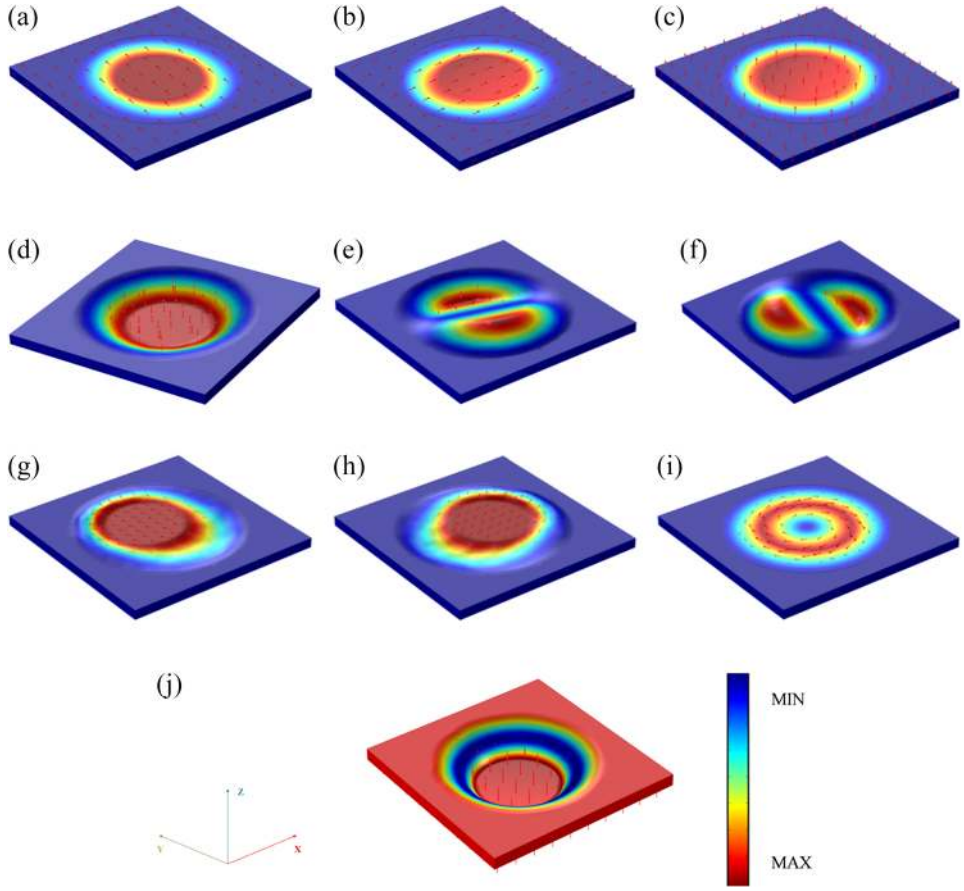

FIG. 8. Displacement vector fields of the vibration modes labeled in Fig. 7. (a) The mode O_1, (b) the mode O_2, (c) the mode O_3, (d) the mode A, (e) the mode B, (f) the mode E, (g) the mode C_1, (h) the mode C_2, (i) the mode D, and (j) the mode F.

coating thickening. As a result, the change of band characteristics is not obvious. However at the post-buckling stage, due to the large thermal deformation, the VMQ coating changes from an annular plate to an approximate truncated conical shell. The stiffness of the mass-spring system along the z direction is enhanced significantly. Hence, the frequencies of mode A and F, which is the upper and lower edges of the Lamb wave bandgap, shifts to higher range abruptly.

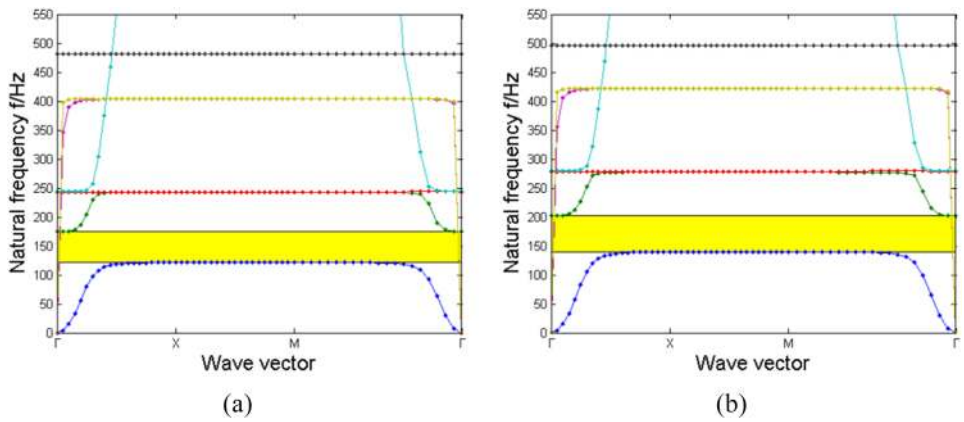

FIG. 9. Band structures of the locally resonant PC plate. (a) At 140°C and (b) at 143°C.

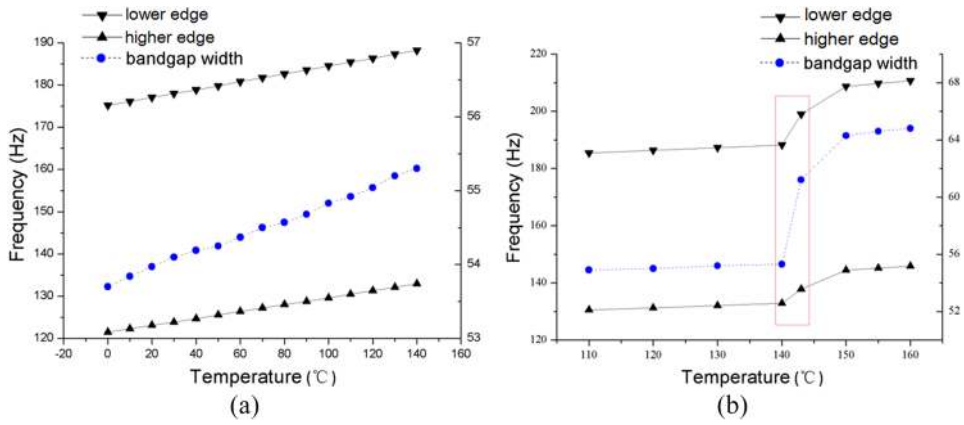

FIG. 10. Evolution of Lamb wave bandgap as a function of the temperature. (a) In the pre-buckling stage and (b) in the post-buckling stage.

IV. CONCLUSIONS AND OUTLOOK

In this paper, the influence of thermal deformation on the bandgap of a ternary phononic crystals structure is studied numerically. Results indicate that the thermal deformation (especially the thermal buckling) has considerable effects on the stiffness of the phononic crystals plate and changes the bandgap. It is found that the bandgap will shift to the higher frequency range as thermal increases. Nevertheless, as the configuration of the VMQ coating changes from an annular plate to an approximate truncated conical shell, the position of bandgap shifts up suddenly at critical buckling temperature. It is obvious that the thermal deformation has a distinct impact on the bandgap of phononic crystals. Hence thermal deformation has to be considered while designing phononic crystals, and also this effect of thermal deformation could be used to tune the bandgap. Ultimately, it is an inevitable challenge to consider both the thermal stress/deformation and the temperature tunable mechanical properties (especially the damping properties) for further research.

ACKNOWLEDGMENTS

The authors gratefully acknowledge the financial support from the Natural Science Foundation of China (No. 11772251) and the 111 Project (B18040).

[1] M. S. Kushwaha, P. Halevi, L. Dobrzynski, and B. Djafari-Rouhani, Physical Review Letters **71**, 2022 (1993).
[2] Z. Liu, X. Zhang, Y. Mao, Y. Zhu, Z. Yang, C. Chan, and P. Sheng, Science **289**, 1734 (2000).
[3] Y. Chen and L. Wang, Applied Physics Letters **105**, 191907 (2014).
[4] Y. Chen, F. Qian, L. Zuo, F. Scarpa, and L. Wang, Extreme Mechanics Letters **17**, 24 (2017).
[5] J. S. Jensen, Journal of Sound and Vibration **266**, 1053 (2003).
[6] G. Wang, X. Wen, J. Wen, L. Shao, and Y. Liu, Physical Review Letters **93**, 154302 (2004).
[7] C. Qiu, Z. Liu, J. Mei, and J. Shi, Applied Physics Letters **87**, 104101 (2005).
[8] J. H. Wen, D. L. Yu, G. Wang, H. G. Zhao, Y. Z. Liu, and X. S. Wen, Physics Letters A **364**, 323 (2007).
[9] T. Wu, L. Wu, and Z. Huang, Journal of Applied Physics **97**, 094916 (2005).
[10] Z. Yan and Y. Wang, Physical Review B **74**, 224303 (2006).
[11] Z. Yan and Y. Wang, Physical Review B **78**, 094306 (2008).
[12] Z. Yao, G. Yu, Y. Wang, and Z. Shi, International Journal of Solids and Structures **46**, 2571 (2009).
[13] C. M. Reinke, M. F. Su, R. H. Olsson III, and I. El-Kady, Applied Physics Letters **98**, 061912 (2011).
[14] J. Y. Yeh, Physica B Condensed Matter **400**, 137 (2007).
[15] Y. Wang, F. Li, W. Huang, X. Jiang, Y. Wang, and K. Kishimoto, International Journal of Solids and Structures **45**, 4203 (2008).
[16] Y. Wang, F. Li, W. Huang, and Y. Wang, Journal of Physics: Condensed Matter **19**, 496204 (2007).
[17] Y. Wang, F. Li, Y. Wang, K. Kishimoto, and W. Huang, Acta Mechanica Sinica **25**, 65 (2009).
[18] Y. Chen, T. Li, F. Scarpa, and L. Wang, Physical Review Applied **7**, 024012 (2017).
[19] Y. Cheng, X. Liu, and D. Wu, Journal of the Acoustical Society of America **129**, 1157 (2011).
[20] Z. J. Chen, Journal of Applied Physics **117**, 124902 (2015).
[21] Y. Liu and Y. Li, Shock and Vibration **20**, 1011 (2013).
[22] W. Li and Y. Li, Acta Mechanica Solida Sinica **28**, 11 (2015).
[23] Q. Geng and Y. Li, Journal of the Acoustical Society of America **135**, 053509 (2014).

[24] D. Flight, M. W. Kehoe, and V. C. Deaton, NASA Technical Memorandum 104269, 1 (1993).
[25] A. Anthoine, International Journal of Solids and Structures **32**, 137 (1995).
[26] Z. Li, X. Wang, and Y. Li, AIP Advances **7**, 015002 (2017).
[27] Q. Geng, D. Wang, Y. Liu, and Y. Li, Science China Technological Sciences **58**, 1414 (2015).
[28] C. Wang, Y. Xu, and J. Du, Materials and Structures **49**, 4867 (2016).
[29] Y. Pennec, B. Djafari-Rouhani, H. Larabi, J. O. Vasseur, and A. C. Hladky-Hennion, Physical Review B **78**, 104105 (2008).
[30] L. Shen, J. Wu, Z. Liu, and G. Fu, International Journal of Modern Physics B **29**, 1550027 (2015).